RESEARCH ARTICLE

Mobocertinib (TAK-788): A Targeted Inhibitor of *EGFR* Exon 20 Insertion Mutants in Non–Small Cell Lung Cancer

Francois Gonzalvez[1], Sylvie Vincent[2], Theresa E. Baker[1], Alexandra E. Gould[2], Shuai Li[3], Scott D. Wardwell[1], Sara Nadworny[1], Yaoyu Ning[1], Sen Zhang[1], Wei-Sheng Huang[1], Yongbo Hu[2], Feng Li[1], Matthew T. Greenfield[1], Stephan G. Zech[1], Biplab Das[1], Narayana I. Narasimhan[1], Tim Clackson[1], David Dalgarno[1], William C. Shakespeare[1], Michael Fitzgerald[2], Johara Chouitar[2], Robert J. Griffin[2], Shengwu Liu[4], Kwok-kin Wong[3], Xiaotian Zhu[1], and Victor M. Rivera[1]

Illustration by Bianca Dunn

ABSTRACT Most *EGFR* exon 20 insertion (*EGFR*ex20ins) driver mutations in non–small cell lung cancer (NSCLC) are insensitive to approved EGFR tyrosine kinase inhibitors (TKI). To address the limitations of existing therapies targeting *EGFR*-mutated NSCLC, mobocertinib (TAK-788), a novel irreversible EGFR TKI, was specifically designed to potently inhibit oncogenic variants containing activating *EGFR*ex20ins mutations with selectivity over wild-type EGFR. The *in vitro* and *in vivo* activity of mobocertinib was evaluated in engineered and patient-derived models harboring diverse *EGFR*ex20ins mutations. Mobocertinib inhibited viability of various EGFRex-20ins-driven cell lines more potently than approved EGFR TKIs and demonstrated *in vivo* antitumor efficacy in patient-derived xenografts and murine orthotopic models. These findings support the ongoing clinical development of mobocertinib for the treatment of *EGFR*ex20ins-mutated NSCLC.

SIGNIFICANCE: No oral EGFR-targeted therapies are approved for *EGFR* exon 20 insertion (*EGFR*ex20ins) mutation-driven NSCLC. Mobocertinib is a novel small-molecule EGFR inhibitor specifically designed to target EGFRex20ins mutants. Preclinical data reported here support the clinical development of mobocertinib in patients with NSCLC with *EGFR* exon 20 insertion mutations.

See related commentary by Pacheco, p. 1617.

INTRODUCTION

Adenocarcinoma, the most common histologic non–small cell lung cancer (NSCLC) subtype (https://seer.cancer.gov/csr/1975_2016), is divided into molecular subtypes with distinct and often actionable oncogenic driver mutations (1). *EGFR* mutations are present in 12% to 38% of lung adenocarcinomas (2, 3) and are more common in patients with NSCLC in East Asia (40%–64%) than in Europe and North America (7%–37%; refs. 4, 5). *EGFR* activating mutations are often found in the first four exons (18 to 21) of the EGFR tyrosine kinase domain (6). Common activating mutations, which account for approximately 78% to 85% of all *EGFR* activating mutations, include exon 19 in-frame deletions and L858R substitution in exon 21 (7–9). First-generation (erlotinib, gefitinib), second-generation (afatinib, dacomitinib), and third-generation (osimertinib) EGFR tyrosine kinase inhibitors (TKI) are approved by the FDA for treatment of patients with metastatic NSCLC with these common mutations and have been associated with high objective response rates (50%–77%; refs. 10–13).

The efficacy of first- and second-generation EGFR TKIs in patients with common activating mutations is impaired by the emergence of drug resistance, which occurs most frequently via acquisition of a secondary mutation, T790M, in the EGFR kinase domain "gatekeeper" residue, impairing drug binding (6, 14). Third-generation TKIs such as osimertinib were developed to address this issue and offer a therapeutic option to patients whose tumors bear combined common and gatekeeper mutations (15). Second- and third-generation TKIs bind irreversibly and covalently to cysteine 797 in the adenosine triphosphate (ATP) binding site of the EGFR kinase (16, 17). Uncommon mutations, which account for approximately 5% of all *EGFR* activating mutations, include point mutations at amino acids in exons 18 (e.g., G719X), 20 (e.g., S768X), and 21 (e.g., L861X; refs. 7, 8). Only afatinib is currently approved by the FDA for use in patients with a specific set of uncommon nonresistant mutations (S768I, L861Q, and G719X; ref. 18); the clinical activity of osimertinib against these mutations is under investigation (19).

The *EGFR* exon 20 insertion (*EGFR*ex20ins) mutation class encodes a family of mutants with amino acid insertions clustered between positions 762 and 774 [e.g., V769_D770insASV (ASV)] that result in constitutive activation of EGFR (20). *EGFR*ex20ins mutations represent approximately 6% to 12% of all *EGFR*-mutated NSCLC cases (7–9, 21) and are enriched in nonsmokers and Asian patients (8, 9). Almost all *EGFR*ex20ins mutations confer *in vitro* and clinical resistance to first- and second-generation EGFR TKIs (7, 8, 20, 22–24), although osimertinib may have clinical efficacy against some resistant mutants (25–28). A small subset of atypical *EGFR*ex20ins mutations [e.g., A763_Y764insFQEA (FQEA)] is associated with sensitivity to first-, second-, and third-generation EGFR TKIs (24, 29). No EGFR TKIs are currently approved for use in patients with *EGFR*ex20ins mutations.

The main challenge of designing TKIs that target EGFRex-20ins mutants is achieving selectivity over wild-type (WT) EGFR (20, 30). Common mutations (L858R, exon 19 deletion) result in EGFR kinases with destabilized inactive forms

[1]ARIAD Pharmaceuticals, Inc., Cambridge, Massachusetts, a wholly owned subsidiary of Takeda Pharmaceutical Company Limited. [2]Millennium Pharmaceuticals, Inc., Cambridge, Massachusetts, a wholly owned subsidiary of Takeda Pharmaceutical Company Limited. [3]Laura and Isaac Perlmutter Cancer Center, New York University School of Medicine, NYU Langone Health, New York, New York. [4]Department of Medical Oncology, Dana-Farber Cancer Institute, Harvard Medical School, Boston, Massachusetts.

Note: Supplementary data for this article are available at Cancer Discovery Online (http://cancerdiscovery.aacrjournals.org/).

Corresponding Author: Victor M. Rivera, Theseus Pharmaceuticals, Inc., 210 Broadway, Suite 201, Cambridge, MA 02139. Phone: 857-206-6967; E-mail: Victor.Rivera@TheseusPharma.com

Cancer Discov 2021;11:1672–87

doi: 10.1158/2159-8290.CD-20-1683

that display reduced ATP affinity relative to WT EGFR (20). First-generation EGFR TKIs take advantage of this difference in ATP affinity to obtain high affinity for mutant EGFR and selectivity over WT EGFR (31, 32). In contrast, structural modeling of EGFRex20ins variants suggests that the insertion of in-frame amino acids at the C-terminal of the C-helix leads to conformational changes closely resembling the active form of WT EGFR, resulting in less selectivity for first- and second-generation EGFR TKIs compared with WT EGFR (20, 24, 33). Inhibition of WT EGFR in normal tissues is associated with dose-limiting toxicities that typically manifest as cutaneous, mucosal, and gastrointestinal adverse events (34–36). EGFR TKIs that inhibit WT EGFR more potently than the targeted oncogenic EGFR mutant are unlikely to allow for dosing at clinically efficacious levels without the development of unacceptable levels of skin and gastrointestinal toxicities (33).

Mobocertinib (TAK-788; AP32788) is a novel oral EGFR TKI that was designed to address the unmet need in patients with EGFRex20ins-mutant NSCLC. Using an iterative, structure-guided strategy, similar to that employed in the development of other targeted TKIs (37), mobocertinib was designed to potently inhibit oncogenic variants containing activating mutations in exon 20, with selectivity over WT EGFR.

RESULTS

Defining the Unmet Need for an EGFR TKI Targeted to EGFRex20ins Mutants

To define the relative incidence of EGFR TKI–resistant *EGFR*ex20ins mutations globally, we extracted data from the American Association for Cancer Research Project Genomics, Evidence, Neoplasia, Information, Exchange (GENIE) database (38). Among 155 patients with lung adenocarcinoma with *EGFR*ex20ins mutations, the most common mutations were A767_V769dup [V769_D770insASV (ASV), 21%], S768_D770dup [D770_N771insSVD (SVD), 18%], and N771_H773dup [H773_V774insNPH D770_N771insNPG (NPH), 9%; Fig. 1A; Supplementary Table S1]. All three *EGFR*ex20ins mutations (ASV, SVD, and NPH) were captured in our screening cascade, as well as D770_N771insNPG (NPG) and FQEA.

To identify an EGFRex20ins inhibitor with the necessary degree of selectivity for mutant EGFR over WT EGFR to be clinically viable, we established an assay that could predict clinical efficacy of first-, second-, and third-generation EGFR TKIs against five classes of EGFR mutants. Activity against WT EGFR was assessed by determining concentrations required to inhibit EGFR phosphorylation in A431 cells, and activity against EGFR mutants was assessed by determining concentrations required to inhibit viability of 15 Ba/F3 cell lines engineered to have their survival dependent on mutant human EGFR activity. We then compared mean erlotinib, gefitinib, afatinib, and osimertinib concentrations required to inhibit WT and mutant EGFR activity by 50% (IC_{50}; Fig. 1B; Supplementary Table S2).

Consistent with their approved indications, all four EGFR TKIs inhibited EGFR with common activating mutations [E746-A750 del (D) and L858R (L)] more potently than WT EGFR, but only osimertinib inhibited T790M-containing mutants [E746-A750 del + T790M (DT) and L858R + T790M (LT)] more potently than WT EGFR. None of the four TKIs inhibited the activity of a triple mutant (L858R + T790M + C797S; LTC), consistent with known clinical resistance mechanisms. Also consistent with their approved indications, afatinib, but not erlotinib or gefitinib, inhibited all five uncommon EGFR mutants more potently than WT (the clinical benefit/risk of osimertinib, which inhibited some but not all uncommon mutants more potently than WT EGFR, is being explored; ref. 19). Importantly, consistent with the lack of meaningful clinical activity, erlotinib, gefitinib, and afatinib all exhibited greatly reduced activity against all five EGFRex20ins mutants (NPG, ASV, NPH, SVD, and FQEA) compared with WT EGFR, except for afatinib against the structurally distinct FQEA mutant. In addition to FQEA, osimertinib inhibited NPG and ASV mutants more potently than WT EGFR but inhibited SVD and NPH mutants less potently than WT. Thus, these models were used to guide discovery of a TKI for patients with *EGFR*ex20ins mutations based on its ability to inhibit all EGFRex20ins mutants more potently than WT EGFR.

Design and Identification of Mobocertinib (TAK-788)

The design and discovery of mobocertinib involved structure-guided design and structure–activity relationship development, including validation of various *in vitro* and *in vivo* nonclinical assays. The conformation of EGFRex20ins mutants largely resembles that of WT EGFR in the ATP binding site (Fig. 2A). With no amino acid substitutions in the binding site, it was challenging to address selectivity directly. However, we adopted an approach to target potential structural nuances between the proteins in the vicinity of the α C-helix to gain selectivity by targeting portions of the binding site not exploited by osimertinib. One such nuance was the observation that, upon NPG insertion, both the P-loop and the C-helix are shifted, making the binding pocket smaller (39).

Like afatinib and osimertinib, mobocertinib was designed to form a covalent interaction with cysteine 797 in EGFR. Compared with a reversible binding mechanism, this irreversible binding mechanism leads to increased potency via higher affinity binding, more sustained EGFR kinase activity inhibition, and greater overall selectivity, as only a limited number of other kinases possess a cysteine in the equivalent position. Amino acid insertion in exon 20 results in a shift of the C-helix to the active conformation of EGFR; this alteration is quite distant from the ATP binding pocket (Fig. 2A–D). An osimertinib docking model in the *EGFR*ex20ins NPG mutant (Fig. 2B) revealed an unoccupied pocket accessible by substitution on the pyrimidine ring. Mobocertinib's isopropyl ester was designed specifically to interact with the gatekeeper residue within this pocket and to probe subtle conformational differences between *EGFR*ex20ins mutants and WT EGFR. This key structural feature results in increased affinity for the *EGFR*ex20ins mutant compared with osimertinib.

An LC/MS study was conducted to determine whether mobocertinib forms an irreversible complex with WT EGFR and an EGFRex20ins mutant. After incubation with mobocertinib, LC/MS analysis revealed a shift in the observed mass of WT and mutant EGFR that corresponded to the exact molecular

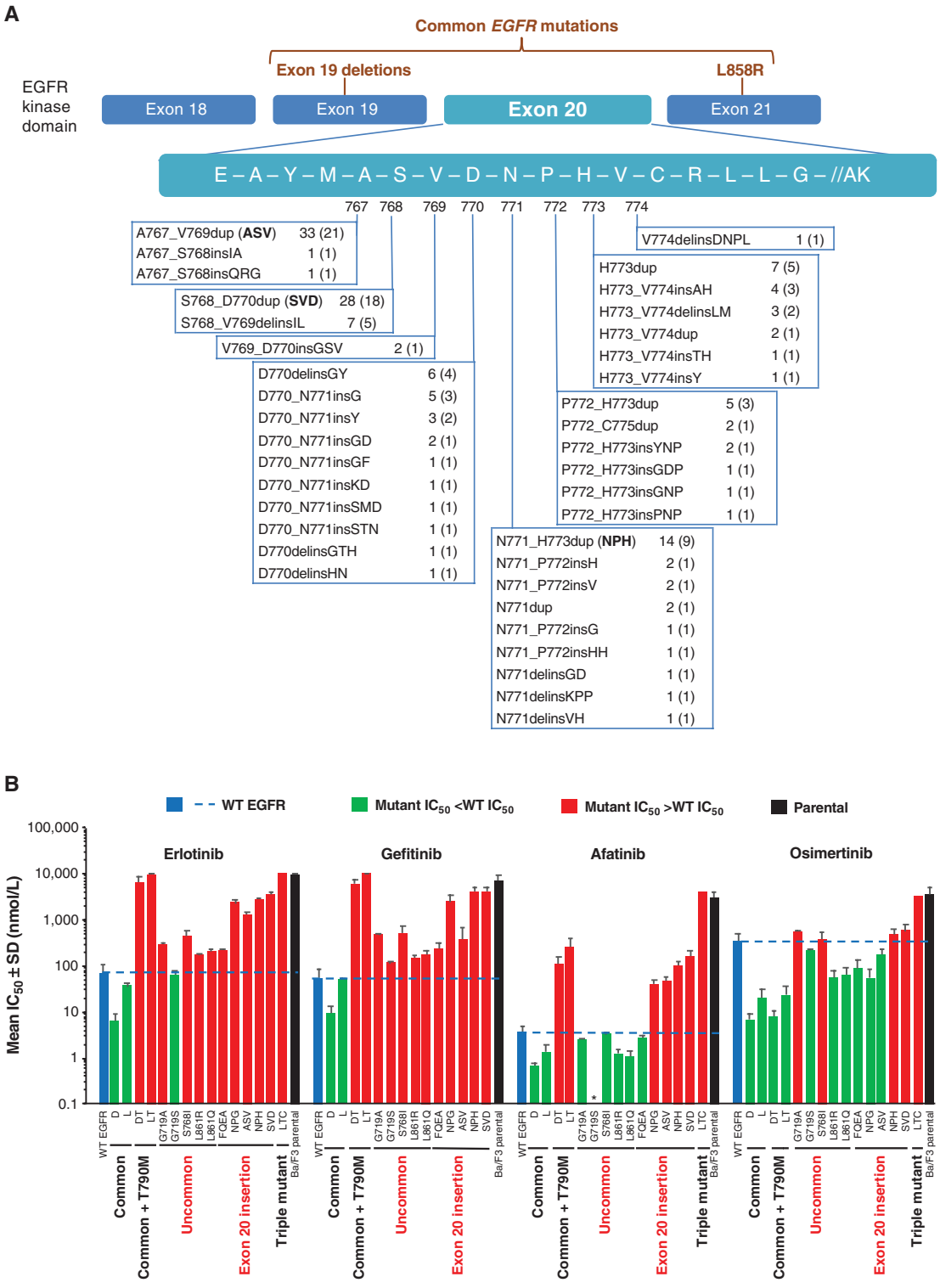

Figure 1. Defining the unmet need for an EGFR TKI targeting *EGFR*ex20ins mutations. **A,** Prevalence of *EGFR*ex20ins mutations in the GENIE database. Data extracted from GENIE v8.0 identified 155 patients with lung adenocarcinoma with *EGFR*ex20ins mutations. TKI-sensitive FQEA mutants are not shown ($n = 5$). Values are number of patients (%). **B,** Development of an assay screening strategy that can predict clinical efficacy based on comparison of inhibitory activity of EGFR TKIs against WT EGFR in A431 cells compared with five classes of human *EGFR*-mutant variants expressed in Ba/F3 cells, which are dependent on the mutant EGFR signaling for viability. *, IC_{50} for afatinib against G719S is <2.4 nmol/L.

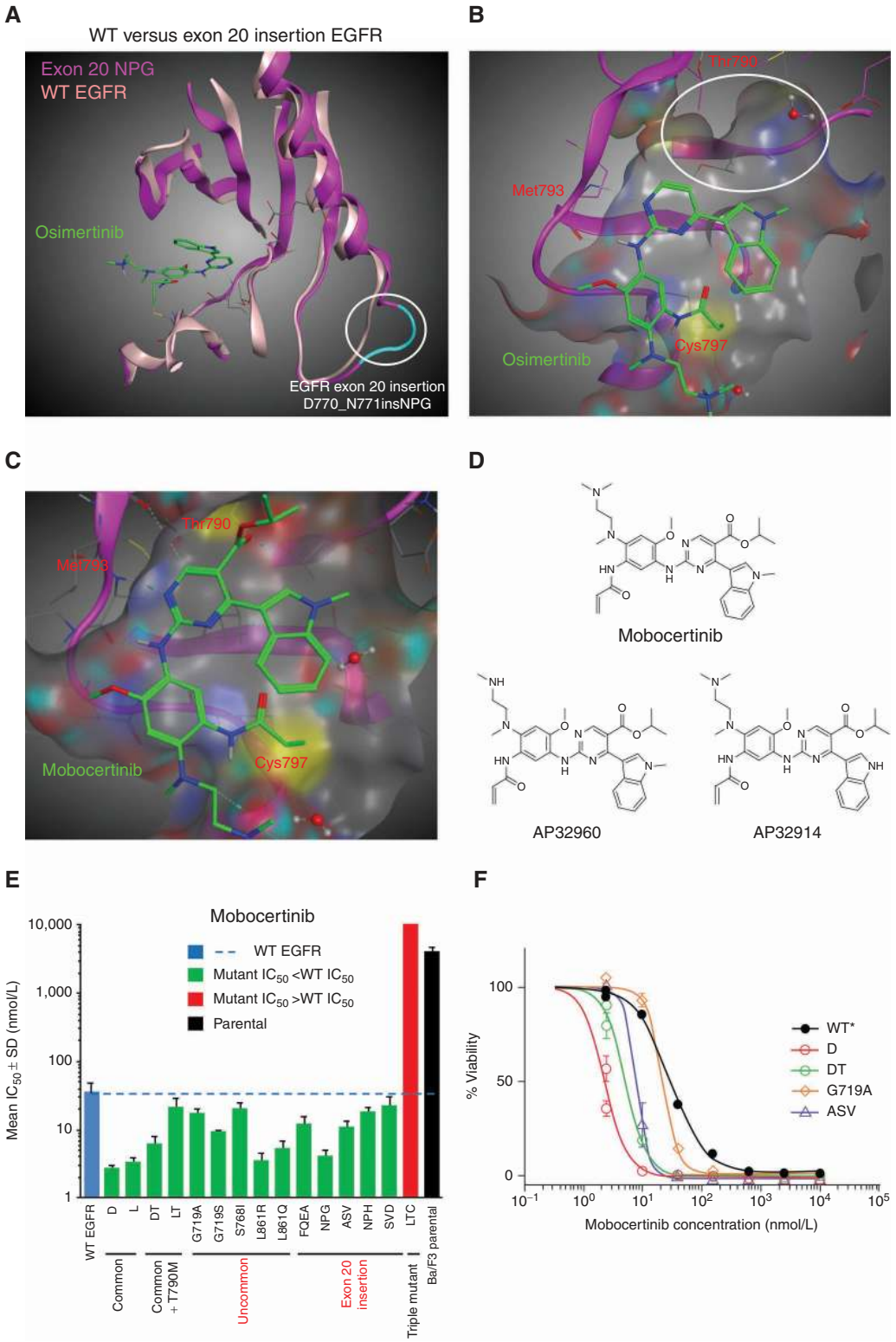

Figure 2. Structure-based drug design and invention of mobocertinib (TAK-788). **A,** Crystal structure of WT EGFR (light pink, PDB code 4ZAU) compared with EGFRex20ins NPG (magenta and cyan, PDB code 7LGS) shows high levels of overlap, especially in the osimertinib binding region. **B,** Model of osimertinib bound to the EGFRex20ins NPG mutant. **C,** Model of mobocertinib bound to EGFRex20ins NPG mutant. **D,** Chemical structure of mobocertinib and two of its metabolites. **E,** Mobocertinib inhibits EGFRex20ins mutants with selectivity against WT EGFR. The graph shows the inhibitory activity of mobocertinib against WT EGFR in A431 cells and against five classes of EGFR mutant, including various EGFRex20ins mutants, in Ba/F3 cells. **F,** Proportional cell viability of Ba/F3 cells harboring D, DT, G719A, and ASV mutants with varying concentrations of mobocertinib. *, Data for WT are pEGFR inhibition data from A431 cells. PDB, Protein Data Bank.

weight of mobocertinib (Supplementary Table S3), demonstrating formation of a covalent, irreversible interaction.

EGFR Inhibitory Profile of Mobocertinib

The inhibitory profile of mobocertinib was evaluated in the Ba/F3 screening assay. Mobocertinib inhibited the activity of 14 of 15 mutant EGFR variants tested (IC_{50}s 2.7–22.5 nmol/L) more potently than WT EGFR (IC_{50} 34.5 nmol/L) (Fig. 2E and F). The only exception was the C797S-containing triple mutant (i.e., LTC; Fig. 2E; Supplementary Table S2), which conferred resistance to mobocertinib (IC_{50} > 10,000 nmol/L). Taken together with the above MS results, this is consistent with its mechanism of covalent binding. Mutants inhibited more potently than WT EGFR included all four variants containing common activating mutations with or without the T790M resistance mutation (D, L, DT, and LT: IC_{50}s 2.7–21.3 nmol/L) and all five variants containing uncommon activating mutations (G719A, G719S, S768I, L861Q, and L861R; IC_{50}s 3.5–20.2 nmol/L). Most importantly, mobocertinib inhibited all five variants containing *EGFR*ex20ins mutations (FQEA, NPG, ASV, NPH, and SVD; IC_{50}s 4.3–22.5 nmol/L) more potently than WT EGFR.

The activity of mobocertinib against EGFRex20ins and other classes of mutants was also assessed in cancer cell lines. To characterize mobocertinib's activity against *EGFR*ex20ins mutations, we used two patient-derived cell lines, CUTO14 and LU0387. CUTO14 cells were derived from the pleural effusion of a patient with lung adenocarcinoma harboring an *EGFR*ex20ins ASV mutation who had no prior TKI treatment (39). LU0387 cells were derived from a patient with lung adenocarcinoma harboring an *EGFR*ex20ins NPH mutation. These cells lack activating mutations in a variety of other potential driver oncogenes (*KRAS*, *ALK*, *BRAF*, *MET*, *PIK3CA*, *AKT*, and *ERK*), consistent with the *EGFR*ex20ins mutation being the primary oncogenic driver. In CUTO14 cells, mobocertinib robustly inhibited EGFR signaling, reaching 80% and 100% inhibition of phosphorylated EGFR (pEGFR) at concentrations of 100 nmol/L and 1,000 nmol/L, respectively, whereas osimertinib induced 38% and 63% inhibition at the same concentrations (Fig. 3A). Mobocertinib inhibited viability of CUTO14 cells (IC_{50} 33 nmol/L) with greater potency than erlotinib, gefitinib, afatinib, and osimertinib (IC_{50}s 2,679, 1,021, 66, and 575 nmol/L, respectively). Mobocertinib inhibited viability of LU0387 cells (IC_{50} 21 nmol/L) with greater potency than WT EGFR phosphorylation (IC_{50} 35 nmol/L) and with potency substantially greater than that of erlotinib, gefitinib, and osimertinib (IC_{50}s 2,793, 364, and 195 nmol/L, respectively; Fig. 3B). Although the potency of afatinib (IC_{50} 20 nmol/L) in LU0387 cells was similar to that of mobocertinib, it had fivefold greater potency against WT EGFR (IC_{50} 3.9 nmol/L) and maximally inhibited LU0387 cell survival by only ≈60%, compared with 85% for mobocertinib.

Inhibitory activity against the most common EGFR activating mutants, with or without a T790M resistance mutation, was assessed by determining concentrations of mobocertinib required to inhibit pEGFR in three NSCLC cell lines expressing EGFR mutants: HCC827 [exon 19 deletion (D)], H4011 [L858R (L)], and H1975 [L858R plus T790M (LT)]. Mobocertinib potently inhibited EGFR with common activating mutations (IC_{50}s 1.3–4.0 nmol/L) or with a T790M mutation (IC_{50} 9.8 nmol/L, LT) more potently than WT EGFR (Fig. 3C). Potent inhibition of EGFR and downstream signaling by mobocertinib were confirmed in all three cell lines by Western blot analysis (Fig. 3D–F).

Examination of the *in vitro* and *in vivo* metabolism of mobocertinib in preclinical studies resulted in the identification of two N-demethylated metabolites (AP32914 and AP32960; Fig. 2D), likely the result of CYP450-mediated oxidative dealkylation. The cellular activities of AP32914 and AP32960 were similar (IC_{50}s typically within twofold) to those of mobocertinib for both WT and mutant EGFR, suggesting the potential for these metabolites to contribute to the pharmacologic activity of mobocertinib (Supplementary Table S2).

Confirmation of Mobocertinib Selectivity in Biophysical and Biochemical Assays

We used a mutant C797S version of *EGFR*ex20ins NPG to evaluate the reversible binding affinity of mobocertinib in a low-temperature Biacore surface plasmon resistance (SPR) assay. Mobocertinib demonstrated substantially better binding affinity to the NPG EGFRex20ins mutant by SPR and better selectivity over WT EGFR compared with osimertinib and afatinib (Fig. 3G). The better selectivity observed upon initial protein-ligand formation is an important factor contributing to the selectivity of mobocertinib toward EGFRex20ins mutants.

The kinase selectivity profile of mobocertinib was evaluated by *in vitro* kinase assays of 490 recombinant human protein kinases (372 unique kinases and 118 mutant variants; Fig. 3H). At 1 μmol/L, mobocertinib inhibited 28 of 490 kinases (6%) by >50%, including all 14 members of the EGFR family tested (EGFR, HER2, HER4, and 11 EGFR variants with activating or resistance mutations; Supplementary Table S4). Dose–response curves were established in a subset of kinases, including the 28 kinases mobocertinib inhibited most potently in the single-point screen and 10 other kinases reported to be involved in critical cellular processes. Of these 38 kinases, 15 were inhibited with IC_{50}s <2 nmol/L, including all 14 members of the EGFR family tested and BLK (Supplementary Table S5). Six additional kinases (JAK3, TXK, BMX, ACK1, BTK, and BTK^{E41K}) were inhibited with IC_{50}s <20 nmol/L. Similar results were obtained with the mobocertinib metabolites AP32914 and AP32960 (Supplementary Table S5). Overall, mobocertinib displayed potent kinase inhibitory activity mainly restricted to the EGFR family of proteins, with limited off-target activity against the rest of the kinome.

Efficacy of Orally Dosed Mobocertinib in EGFR-Mutant Tumor Models

We evaluated mobocertinib in two mouse tumor models containing an *EGFR*ex20ins ASV mutation. In a tumor model using engineered Ba/F3 cells, once-daily oral dosing of mobocertinib showed dose-dependent inhibition of tumor growth, or tumor regression, at well-tolerated doses (Supplementary Fig. S1A and S1B). In a xenograft model using CTG-2842 cells from a patient with *EGFR*ex20ins ASV-mutant NSCLC who had been treated with erlotinib (without response), mobocertinib dosed orally at 15 mg/kg daily induced substantial tumor regression (92%; Fig. 4A) and was well tolerated (Supplementary Fig. S2).

A

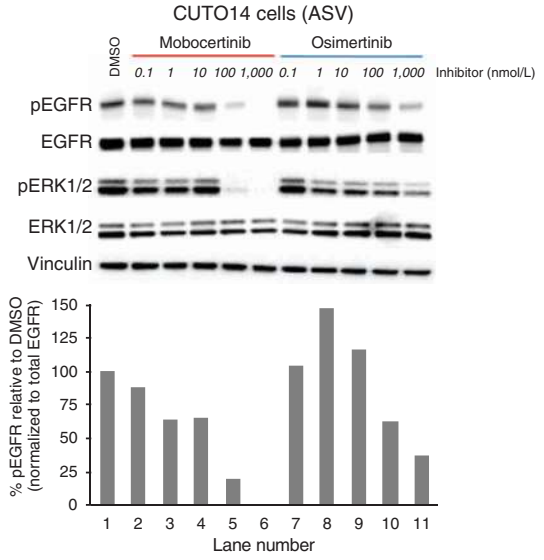

B

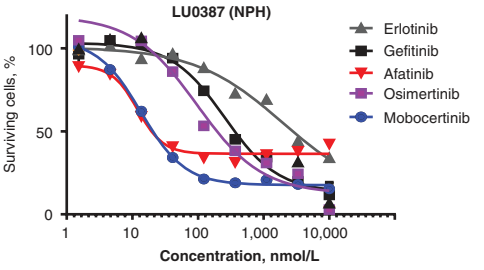

LU0387 (NPH)	IC_{50} (nmol/L)
Erlotinib	2,793
Gefitinib	364
Afatinib	20
Osimertinib	195
Mobocertinib	21

C

pEGFR inhibition in NSCLC cell lines (mean IC_{50}s ± SD [nmol/L])*

	A431	HCC827	HCC4011	H1975
	WT	D	L	LT
Erlotinib	71 ± 54	6.7 ± 3.6	17 ± 2	245
Gefitinib	56 ± 38	4.1 ± 2.9	11 ± 1	2560
Afatinib	3.9 ± 1.3	1.4 ± 0.5	0.3 ± 0.0	8.9 ± 3.4
Mobocertinib	35 ± 18	4.0 ± 2.2	1.3 ± 0.4	9.8 ± 5.4

D

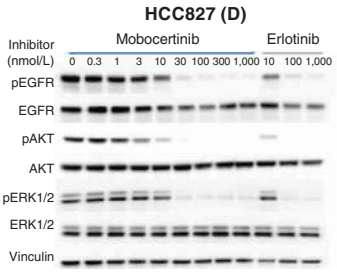

E

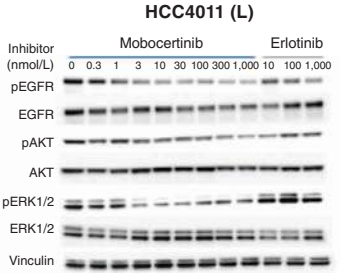

F

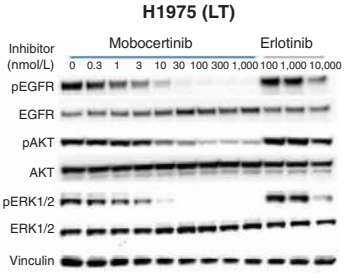

G

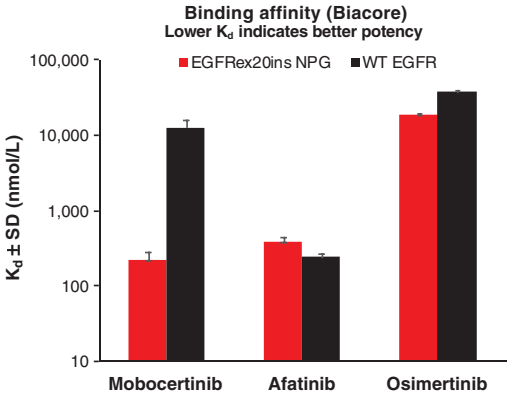

H

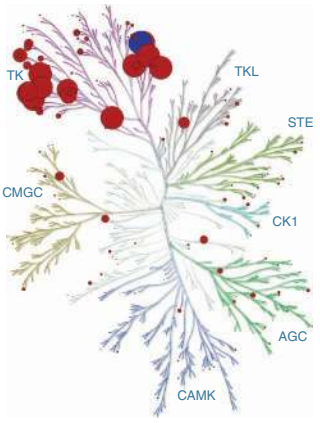

We next investigated antitumor activity of oral mobocertinib in mice engrafted with LU0387 tumors expressing an EGFRex20ins NPH mutant. At 10 mg/kg daily, mobocertinib induced 56% tumor growth inhibition, and at 30 mg/kg daily induced 87% tumor regression relative to pretreatment tumor size ($P < 0.0001$; Fig. 4B). In contrast, erlotinib induced 38% tumor growth inhibition at 50 mg/kg. Significant inhibition of tumor growth was also achieved with osimertinib 30 mg/kg daily, although to a lesser degree (mean 13% tumor regression; 3/10 mice with >50% regression) than that achieved with an equivalent dose of mobocertinib (mean 87% tumor regression; 10/10 mice with >50% regression; Fig. 4B). The 10- and 30-mg/kg daily doses of mobocertinib were well tolerated (Supplementary Fig. S3A) with no clinical signs or drug-related mortality. Increased efficacy was associated with increased plasma levels of mobocertinib and its active metabolites (Supplementary Fig. S3B). Pharmacodynamic activity of mobocertinib was assessed by measuring the levels of pEGFR (Tyr 1068) in LU0387 tumors. Representative Western blot experiments are shown in Fig. 4C. There was no substantial impact on pEGFR levels in mice treated with 10 mg/kg mobocertinib or 50 mg/kg erlotinib, doses associated with relatively modest tumor growth inhibition. At 30 mg/kg, the dose associated with 87% tumor regression, mobocertinib strongly inhibited tumor pEGFR levels. These data demonstrating dose-dependent pEGFR inhibition in tumors indicate that mobocertinib suppressed growth of EGFRex20ins mutant tumors through EGFR inhibition. Combination treatment with mobocertinib and cetuximab improved efficacy in a head and neck squamous cell carcinoma model (CTG-2130) with *EGFR*ex20ins D770_N771insGL (Fig. 4D).

Mobocertinib showed robust antitumor efficacy and was well tolerated in tumor models driven by other EGFR mutations, including the PC9 xenograft model harboring the common exon 19 deletion (D; Supplementary Fig. S4A and S4B) and the H1975 xenograft model harboring the LT mutation (Fig. 4E; Supplementary Fig. S5A and S5B). Mobocertinib demonstrated minimal efficacy in a brain metastasis model in mice intracranially implanted with H1975-luc tumors (Supplementary Fig. S6).

In Vivo Antitumor Efficacy of Mobocertinib in an EGFRex20ins Mutant Lung Cancer Genetically Engineered Mouse Model

To further evaluate mobocertinib efficacy against EGFRex20ins expressing tumors *in vivo*, we generated a genetically engineered mouse model (GEMM) with inducible expression of human *EGFR* D770_N771insSVD (SVD). We electroporated mouse embryonic stem (ES) cells with a DNA construct containing LoxP–Stop–LoxP–hEGFR SVD and injected these positive ES cells into blastocysts to produce chimeras. The chimera mice were further crossed with WT mice to generate germlines. We intranasally delivered adeno-Cre virus into adult *EGFR*ex20ins SVD mice to initiate EGFRex20ins SVD expression specifically in murine lung epithelial cells (Fig. 5A). MRI monitoring showed that lung tumors appeared 14 weeks after viral delivery (Fig. 5B). Immunohistochemistry staining demonstrated that SVD-expressing tumors were positive for adenocarcinoma markers thyroid transcription factor 1 (TTF1) and surfactant protein C (SPC), as well as negative for the squamous cell carcinoma marker p63 (Fig. 5C), indicating that this model mimicked the clinical setting, as most *EGFR*-mutant lung tumors are adenocarcinomas. Long-term monitoring showed the growth kinetics of these tumors (Fig. 5B) and indicated that mice had a median survival time of 21.7 weeks after adeno-Cre induction (Fig. 5D).

To investigate the short-term efficacy of mobocertinib, we performed a pharmacodynamic study in tumor-bearing *EGFR*ex20ins SVD mice. After 1 week of treatment, mobocertinib-treated SVD mice had significantly reduced tumor volumes compared with those treated with vehicle control (Fig. 5E). We harvested lung tumors and stained tissues for pEGFR and pERK1/2. Immunohistochemistry results demonstrated that mobocertinib effectively abolished pEGFR and inhibited its major downstream signaling target pERK (Fig. 5F), supporting the on-target efficacy of mobocertinib against *EGFR*ex20ins SVD *in vivo*.

Next, we treated *EGFR*ex20ins SVD mice with continuous mobocertinib or vehicle and evaluated long-term antitumor efficacy by MRI every 2 weeks. Vehicle-treated mice developed progressive disease at 2 and 4 weeks. In contrast, all mobocertinib-treated mice ($n = 8$) showed significant tumor growth inhibition, with up to a 90% decrease from baseline in tumor volume (Fig. 5G and H), with responses sustained for 10 weeks (Fig. 5I). These studies demonstrated a sustained benefit of mobocertinib for EGFRex20ins SVD tumors, which was consistent with the early observed efficacy and pharmacodynamic results. Taken together, these data indicated that mobocertinib has on-target, efficacious, and durable antitumor effects in *EGFR*ex20ins SVD lung cancer.

DISCUSSION

EGFRex20ins-mutant NSCLC is a life-threatening disease involving rare mutations for which no currently approved oral EGFR-targeted therapy is available. Mobocertinib is an irreversible TKI specifically designed to address this need. We demonstrated that mobocertinib

Figure 3. Characterization of mobocertinib activity and selectivity. **A,** Western blot of total EGFR and pEGFR and ERK1/2 following incubation of patient-derived CUTO14 cells (ASV) with varying concentrations of mobocertinib or osimertinib. **B,** Viability of patient-derived LU0387 (NPH) cells in the presence of different EGFR inhibitors. **C,** Inhibitory activity of mobocertinib and other EGFR inhibitors on EGFR phosphorylation in NSCLC cell lines. *, Number of experimental repetitions for erlotinib and gefitinib versus A431, $n = 7$; HCC827, $n = 2$; HCC4011, $n = 2$; H1975, $n = 1$; afatinib versus A431, $n = 26$; HCC827, $n = 2$; HCC4011, $n = 2$; H1975, $n = 5$; mobocertinib versus A431, $n = 22$; HCC827, $n = 2$; HCC4011, $n = 2$; H1975, $n = 9$. **D–F,** Representative Western blots comparing inhibition of EGFR-mediated signaling in NSCLC cell lines by mobocertinib and erlotinib. **G,** Binding affinity (K_d) of osimertinib, mobocertinib, and afatinib in a Biacore SPR assay. **H,** Kinase tree showing percentage inhibition of each kinase by 1 μmol/L mobocertinib at 10 mmol/L ATP. Circle size is proportional to percentage inhibition. EGFR is represented by a blue circle and all other kinases are red. Kinome tree illustration reproduced courtesy of Cell Signaling Technology, Inc.

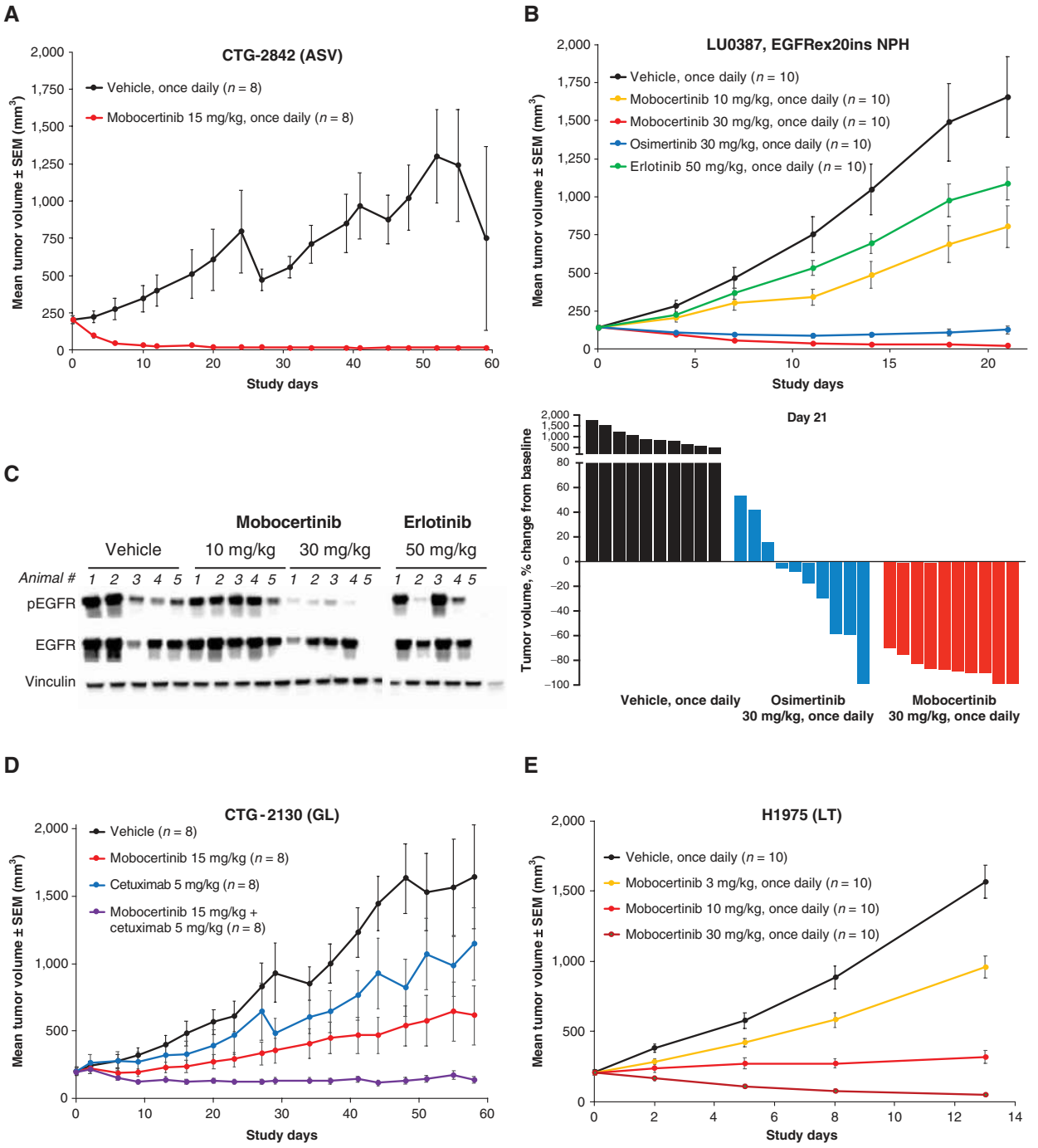

Figure 4. Orally dosed mobocertinib is highly efficacious in multiple *EGFR*-mutant xenograft models. **A,** Tumor volume in a patient-derived xenograft CTG-2842 (ASV) NSCLC tumor model in mice. Among the eight mice in the vehicle group, six were lost to tumor progression during the study: two at day 25, one each at days 42 and 52, and two at day 55. At 15 mg/kg once daily, mobocertinib demonstrated 92% tumor regression at day 59 (growth inhibition of 250% relative to the vehicle group; 95% CI, 131–370%; $P = 0.001$). All mice treated with mobocertinib 15 mg/kg once daily were alive at day 59. **B,** Mean and percent change from baseline in tumor volume in mice engrafted with LU0387 tumors expressing the *EGFR*ex20ins NPH mutant who were administered vehicle, mobocertinib, osimertinib, or erlotinib orally once daily for 21 consecutive days. **C,** pEGFR levels in LU0387 *EGFR*ex20ins NPH xenograft tumors in mice dosed orally with mobocertinib or erlotinib for 21 days. **D,** Tumor volume in mice bearing head and neck tumor xenograft model CTG-2130 bearing *EGFR*ex20ins D770_N771insGL (GL). Mobocertinib 15 mg/kg once daily alone resulted in significant antitumor activity compared with vehicle treatment (growth rate inhibition: 64%, $P < 0.001$). Cetuximab 5 mg/kg once every 3 days alone resulted in nonsignificant antitumor activity compared with vehicle (growth rate inhibition: 21%; $P = 0.141$). The combination of mobocertinib and cetuximab resulted in growth rate inhibition of 109% ($P < 0.001$) compared with vehicle. **E,** Tumor volume in a human NSCLC H1975 LT tumor model in mice. Mobocertinib significantly reduced H1975 tumor growth at all dose levels ($P < 0.0001$). At 3 mg/kg and 10 mg/kg, mobocertinib decreased the mean tumor volume by 44% and 92%, respectively, relative to the tumor size of vehicle group. At 30 mg/kg, mobocertinib induced a 76% tumor regression relative to the pretreatment tumor size.

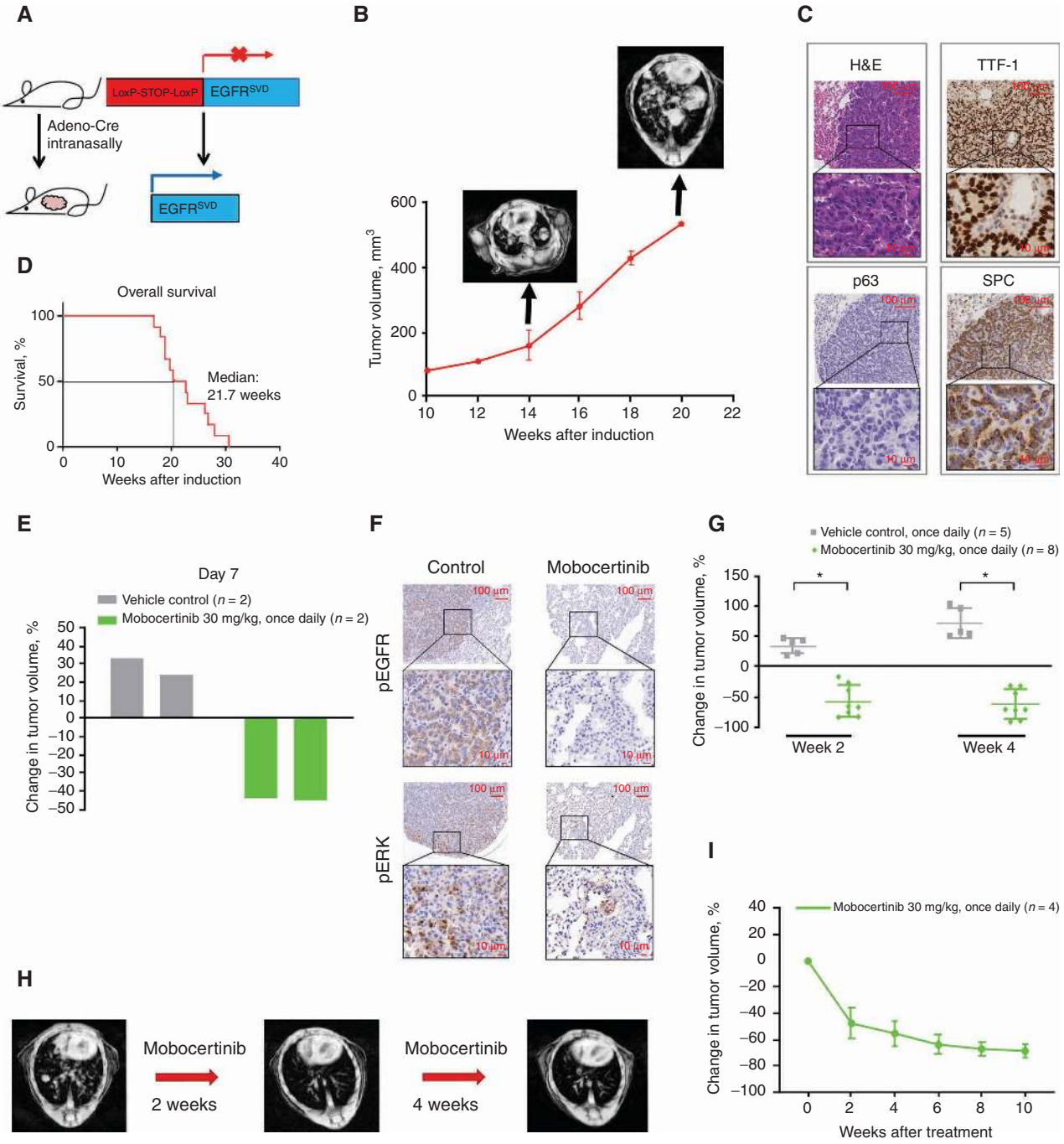

Figure 5. *In vivo* efficacy of mobocertinib in orthotopic *EGFR*ex20ins SVD GEMM of lung cancer. **A,** Schematic of transgene insertion strategy to generate inducible LSL-*EGFR*ex20ins SVD (*EGFR*^{SVD}) mutant mice via intranasal adeno-Cre induction. **B,** Tumor growth curve based on MRI results of *EGFR*ex20ins SVD mutant lung tumors after adeno-Cre induction ($n = 2$) and representative MRI images of *EGFR*ex20ins SVD mutant mice 14 or 20 weeks after adeno-Cre induction. **C,** Representative immunohistochemistry staining images of *EGFR*ex20ins SVD mutant tumors with hematoxylin and eosin (H&E), TTF-1, p63, and SPC. Scale bars, 100 μm or 10 μm. **D,** Overall survival of *EGFR*ex20ins SVD mutant mice after adeno-Cre induction ($n = 12$). **E,** Waterfall plot showing percentage change from pretreatment in tumor volume in *EGFR*ex20ins SVD mutant mice treated with mobocertinib 30 mg/kg once daily or vehicle control for 1 week. Each bar represents one mouse. **F,** Representative immunohistochemistry staining images of pEGFR and pERK1/2 in lung tissues of *EGFR*ex20ins SVD mutant mice. Scale bars, 100 μm or 10 μm. **G,** Volume change of *EGFR*ex20ins SVD mutant tumors 2 and 4 weeks after initiation of treatment with mobocertinib or vehicle control. Each dot represents one mouse. *, $P < 0.0001$. **H,** Representative MRI images of *EGFR*ex20ins SVD mutant mice before and after treatment with mobocertinib for 2 and 4 weeks. **I,** Long-term monitoring of tumor volume change with mobocertinib treatment in *EGFR*ex20ins SVD mutant mice. TTF-1, thyroid transcription factor 1.

has better potency and selectivity over WT EGFR for all EGFRex20ins mutants tested (IC_{50}s 4.3–22.5 nmol/L) than erlotinib, gefitinib, afatinib, and osimertinib. Mobocertinib also demonstrated potent activity against EGFR with common activating mutations with or without the T790M resistance mutation (D, L, DT, and LT: IC_{50}s 2.7–21.3 nmol/L) and uncommon activating mutations (G719A, G719S, S768I, L861Q, and L861R; IC_{50}s 3.5–20.2 nmol/L). Mobocertinib inhibited all three classes of mutants with potency greater than WT EGFR, although it is unclear whether the degree of selectivity is greater than that observed for EGFR TKIs approved for patients with these mutations. In addition, mobocertinib showed robust efficacy in tumor models harboring common exon 19 deletion (D) and T790M mutations. These results are consistent with those of previous studies reporting that mobocertinib inhibits T790M and L858R mutants, as well as *EGFR*ex20ins ASV, SVD, FQEA, and H773_V774insH mutants in Ba/F3 cells, more potently than WT EGFR (40). Mobocertinib also demonstrated dose-dependent inhibition of cell viability in patient-derived cancer cell lines bearing FQEA or N771_H772insH mutations in previous studies (40). The consistent selectivity for a broad range of mutant EGFR variants over WT EGFR suggests that mobocertinib may have lower potential for dose-limiting toxicities associated with EGFR inhibition in normal tissues (e.g., skin and gastrointestinal adverse events) than drugs with less selectivity for these mutants, although gastrointestinal and skin adverse events were reported in the phase I/II trial (41).

Mobocertinib was well tolerated and demonstrated sustained dose-dependent inhibition of tumor growth in both patient-derived xenografts and murine orthotopic models of NPH, ASV, and SVD *EGFR*ex20ins-mutant NSCLC. Both mobocertinib and osimertinib induced tumor regression in the LU0387 NPH tumor model, but the extent of regression was greater with mobocertinib 30 mg/kg daily (87%) compared with osimertinib 30 mg/kg daily (13%). Combination treatment with mobocertinib plus cetuximab improved efficacy in a head and neck cancer model with an *EGFR*ex20ins mutation (D770_N771insGL) that was less sensitive to mobocertinib, consistent with results for afatinib or osimertinib in combination with cetuximab in D770_N771insNPG *EGFR*ex20ins mutant cell lines (42).

Similar to our data, prior studies have demonstrated that osimertinib potently inhibits some EGFRex20ins mutants in Ba/F3 cells (25). However, osimertinib demonstrated limited clinical activity (objective response rate, 5%) in patients with *EGFR*ex20ins NSCLC at the approved dose (80 mg/d; ref. 43); a higher dose (i.e., 160 mg/d) may be needed for substantial efficacy in patients with *EGFR*ex20ins mutations (26–28).

Other novel EGFR TKIs (e.g., poziotinib, TAS6417/CLN-081, DZD9008, tarloxotinib, and DS-2087b) have demonstrated preclinical activity and are under investigation in *EGFR*ex20ins-mutated NSCLC (39, 44–49). Poziotinib demonstrated limited efficacy in patients with *EGFR*ex20ins mutations, and doses of 16 mg/d or less were associated with high rates of WT EGFR-mediated toxicity and dose reduction (48, 49). Tarloxotinib did not demonstrate any objective responses among 11 patients with *EGFR*ex20ins mutations in a phase II trial (46). Preclinical and clinical data suggest that amivantamab, a bispecific antibody that targets EGFR and MET, may have efficacy for patients with NSCLC with *EGFR*ex20ins mutations (50–52).

In conclusion, our preclinical data demonstrated that mobocertinib is a pan-mutation-selective irreversible EGFR TKI with a broad spectrum of *in vitro* and *in vivo* activity against clinically relevant *EGFR* mutations, including several of the most common *EGFR*ex20ins mutations. Based on its favorable preclinical pharmacokinetic (PK) and toxicity profile, mobocertinib was selected for clinical development as a treatment for patients with *EGFR*ex20ins-mutated NSCLC. Mobocertinib demonstrated antitumor activity in patients with NSCLC with diverse EGFRex20ins variants with a safety profile consistent with other EGFR inhibitors in the first two parts of a three-part phase I/II study (ClinicalTrials.gov identifier: NCT02716116). The phase I/II results are reported in a companion article in this issue by Riely and colleagues (53).

METHODS

GENIE Database Search for EGFRex20ins Mutations in NSCLC

Data from GENIE v8.0 (38) were extracted for patients with *EGFR* mutation in all cancer types. Only tumors with in-frame insertions and insertion–deletions in EGFR were considered; excluding pathologies other than lung cancer resulted in identification of 226 data points. After removal of duplicate data, 157 patients with *EGFR* insertions or insertion–deletions were identified; 155 patients had an insertion/insertion–deletion in the exon 20 coding region (amino acids 763–775).

Ba/F3 and A431 Cell Assays

All cell lines were grown at 37°C, with 5% CO_2, in medium supplemented with 10% FBS. Sources of cell lines, growth medium, and additional supplements used are as follows: A431 cells (ATCC; RPMI 1640 growth medium), HEK293 cells (Thermo Fisher Scientific; DMEM growth medium), and parental Ba/F3 cells (German Collection of Microorganisms and Cell Cultures GmbH; RPMI 1640 growth medium supplemented with 10 ng/mL IL3). Per standard protocol, all Ba/F3 EGFR mutants and A431 cells were tested and negative for *Mycoplasma*. Mobocertinib, AP32914, AP32960, erlotinib, gefitinib, afatinib, and osimertinib were synthesized at ARIAD Pharmaceuticals, Inc., or purchased from commercial sources.

Cloning of human EGFR-mutant coding sequence into the pLVX.IRES.Puro lentiviral vector (Takara Bio USA) was performed by GenScript. All cloned genes were confirmed by sequencing. Viral particles were produced by transfecting pLVX.IRES.Puro vectors into HEK293 cells using the Trans-Lentiviral ORF Packaging Kit (GE Healthcare). Forty-eight hours posttransfection, virus-containing supernatants were harvested and incubated for another 48 to 72 hours with parental Ba/F3 cells in the presence of IL3. Transduced Ba/F3 cells were then selected with puromycin (0.5 μg/mL). Upon reaching confluence, cells were grown in IL3-deprived medium to render them solely dependent on transduced *EGFR*-mutant gene activity for survival.

Survival Assay in Ba/F3 Stable Cells Expressing EGFR-Mutant Proteins. Cells were plated and incubated with compound, in

duplicate, using a Tecan HP D300 Instrument (Tecan), for 3 days at 37°C. Cell viability was measured using Cell Titer-Glo assay (Promega). Dose–response curves were generated and used to calculate IC_{50} values.

Measuring WT EGFR Activity in A431 Cells. The potency with which compounds inhibited WT EGFR activity was assessed by measuring levels of EGFR phosphorylated at Tyr1068 (pEGFR) in *EGFR*-amplified A431 (epidermoid carcinoma) cells. A431 cells were incubated with compound for 2 hours and stimulated for 20 minutes with EGF (25 ng/mL), and lysates were prepared. Total EGFR and pEGFR levels in lysates were simultaneously measured by immunoassays using the Meso Scale Discovery Multi-Array platform [Meso Scale Discovery (MSD)] per the manufacturer's protocol. IC_{50}s for inhibition of WT EGFR activity were calculated by examining levels of pEGFR normalized to total EGFR levels in dose–response curves.

LC/MS Detection of Mobocertinib Complex with Mutant or WT EGFR Protein

Avi-tagged constructs *EGFR* WT-Avi and *EGFR*ex20ins NPG-Avi were expressed in baculovirus, enzymatically biotinylated, and incubated with ≈80 μmol/L mobocertinib under conditions maintaining native fold. After a 30-minute incubation, the mixture was subjected to LC/MS analysis under denaturing conditions. Liquid chromatography was performed using a POROS R2/20 2.1-mm × 30-mm column (Applied Biosystems, Thermo Fisher Scientific; mobile phase A: 0.1% formic acid in water, mobile phase B: 0.1% formic acid in acetonitrile; flow rate, 0.5 mL/min). LC/MS experiments were conducted using a Xevo G2-S QTof mass spectrometer equipped with an Acquity UPLC (Waters Corporation) under positive ion mode. Full-scan (200–2,000 *m/z*) electrospray ionization and MS data were collected at a resolution of 32,500 at full width at half maximum (FWHM) using MassLynx software version 4.1 (Waters Corporation).

Assays in NSCLC Cell Lines

Cell Lines and Culture Conditions. HCC4011 cells (UT Southwestern) and HCC827 and H1975 cells (ATCC) were maintained in RPMI 1640 medium. LU0387 primary cells (Crown Bioscience) were maintained in DMEM Nutrient Mixture F-12 growth medium. CUTO14 cells (University of Colorado, Aurora) were maintained in RPMI 1640 growth medium. All cell lines were grown at 37°C, with 5% CO_2, in medium supplemented with 10% FBS. CUTO14 cells tested negative for *Mycoplasma* and were authenticated by short-tandem repeat profiling at the source laboratory prior to freezing and shipment to Takeda. For *in vitro* and *in vivo* experiments, cells were used between passages 3 and 20. Per standard protocol, all HCC827 and HCC4011 cells were tested and negative for *Mycoplasma*.

Cell Viability Assay. Viability assays using LU0387 cells were performed at Crown BioScience. Cells were plated into 96-well plates and dosed with a nine-point, threefold dilution series of compounds (10 μmol/L to 1.5 nmol/L) and incubated for 7 days. Viability was measured using the CellTiter-Glo assay (Promega). Dose–response curves were generated and used to calculate IC_{50} values.

pEGFR Western Blotting. The potency with which compounds inhibited pEGFR signaling was assessed in CUTO14, HCC827, H4011, and H1975 cells by incubating them with compound (CUTO14: mobocertinib or osimertinib at concentrations of 0.1–1,000 nmol/L; HCC827, HCC4011, and H1975 cells: erlotinib 10–1,000 or 100–10,000 nmol/L, or mobocertinib 0.3–1,000 nmol/L) for 6 hours and evaluating levels of pEGFR in cellular lysates using Western blotting for pEGFR, EGFR, pERK1/2, ERK1/2, pAKT, and AKT with antibodies from Cell Signaling Technology [pAKT (Ser473) (D9E) XP rabbit monoclonal antibody (mAb) #4060; AKT antibody rabbit #9272; EGFR (D38B1) XP rabbit mAb #4267; pEGFR (Tyr1068) (D7A5) XP rabbit mAb #3777; p-p44/42 MAPK (ERK1/2) (Thr202/Tyr204) (D13.14.4E) XP rabbit mAb #4370; p44/42 MAPK (ERK1/2) (137F5) rabbit mAb #4695; and Vinculin (E1E9V) XP rabbit mAb #13901].

pEGFR Immunoassays. NSCLC cells were treated with compound for 2 hours, then lysed in a Multi-Array platform (MSD) lysis buffer. Total EGFR and pEGFR (Tyr1068) levels were measured using the MSD Multi-Array immunoassay system. EGFR phosphorylation ratios (pEGFR/total EGFR) were calculated and used to determine dose–response curves and IC_{50}s using GraphPad Prism (GraphPad Software).

Biacore SPR Assay

Measurement of WT and *EGFR*ex20ins NPG EGFR binding affinities was performed using SPR [Biacore T200 using a CM5 chip (Cytiva); chip compartment temperature 10°C; sample compartment temperature, 20°C) in the presence of different concentrations of mobocertinib, afatinib, and osimertinib to assess dissociation constants (K_d). The EGFR proteins used were truncated versions of EGFR containing a C797S mutation and had an AviTag (Avidity LLC) appended to the C-terminal end. An amine coupling was performed by injecting a mixture of 1-ethyl-3-(3-dimethylaminopropyl)carbodiimide (EDC) and N-hydroxysuccinimide (NHS) followed by injection of NeutrAvidin (Thermo Fisher Scientific) and capping the chip with ethanolamine. The two EGFR proteins were immobilized by injecting a solution of the protein typically diluted to 1 mg/mL of the running buffer (25 mmol/L HEPES, pH 7.4; 250 mmol/L NaCl; 10% glycerol; 2 mmol/L Tris (2-carboxy-ethyl)-phosphin-HCl; 0.1% CHAPS; 1% trehalose; 2% DMSO), and then the chip was capped with 1 mmol/L solution of biotin in running buffer. K_d values were determined using the T200 Software Biacore package (Cytiva).

Kinase Assay

In vitro profiling of the 490-member kinase panel was performed at Reaction Biology Corporation using the Kinase HotSpot platform. First, a broad panel of 490 protein kinases, including 372 unique human kinases and an additional 118 mutant variants, was assayed using a single mobocertinib concentration of 1 μmol/L. A second screen was performed on a panel of 38 kinases, including 28 kinases inhibited most strongly in the first assay and 10 additional kinases of interest using a broad range of mobocertinib, AP32914, and AP32960 concentrations to allow determination of IC_{50} values. Percentage inhibition data for each kinase was mapped to the kinome tree (54) using Kinome Render (55).

Tumor Models in Mice

CTG-2842 and CTG-2130 Xenograft Models. CTG-2842 cells (Champions Oncology) are derived from a lung adenocarcinoma, established from the primary site of a patient previously treated with carboplatin/pemetrexed with response and subsequent progression at 6 months, with erlotinib with no response, and with pembrolizumab/coxsackievirus with no response. CTG-2130 cells (Champions Oncology) are derived from a head and neck squamous cell carcinoma, established from a skin metastasis of a patient who was previously treated with and had no response to cisplatin and cetuximab; subsequently, the patient was treated with and had no response to an anti–PD-L1 inhibitor/anti-LAG3 inhibitor and paclitaxel. Tumor fragments generated from CTG-2842 cells or CTG-2130 cells were inoculated subcutaneously into the left flank of female athymic Nude-Foxn1nu mice (Envigo). When average

tumor volume reached 150 to 300 mm^3, animals were treated with vehicle or mobocertinib 15 mg/kg orally daily ± cetuximab 5 mg/kg i.p. once every 3 days for up to 60 days. Tumor size was measured twice weekly.

EGFRex20ins ASV Ba/F3 Tumor Model. Ba/F3 cells expressing *EGFR*ex20ins ASV were used to generate subcutaneous tumors in severe combined immunodeficiency disease (SCID) mice (8 weeks old; Charles River Laboratories). When the average tumor volume reached about 150 mm^3, animals were treated with vehicle or mobocertinib 30 or 50 mg/kg by oral gavage once daily for 7 days. Tumor size was measured at least twice a week. Mice were euthanized on day 7 at 2, 6, or 24 hours after the last dose, when blood samples were collected for PK analysis.

LU0387 Xenograft Model. Female Nu/Nu mice (Beijing Vital River Laboratory Animal Technology Co., Ltd) were inoculated subcutaneously in the right flank with one LU0387 tumor fragment (2–3 mm in diameter; Crown Bioscience). When average tumor volume reached 150 mm^3, animals were treated with vehicle, mobocertinib 10 or 30 mg/kg, erlotinib 50 mg/kg, or osimertinib 30 mg/kg once daily for 21 days. Tumor size was measured every 3 days. Mice were euthanized on day 21, 2 or 6 hours after the last dose, and blood samples were collected for PK analysis. LU0387 tumor samples were homogenized in RIPA buffer and analyzed by Western blotting with antibodies against total EGFR and pEGFR that recognize EGFR tyrosine 1068 (Cell Signaling Technology) and β-actin (Sigma).

PC9 (Exon 19 Deletion) Xenograft Model. Female nude BALB/c mice (Beijing Vital River Laboratory Animal Technology Co., Ltd) were injected subcutaneously with a suspension of 2.0×10^6 PC9 human lung adenocarcinoma cells. When the mean tumor volume reached approximately 240 mm^3, mice were orally dosed with vehicle or mobocertinib 10 or 30 mg/kg once daily for 21 days. Tumor growth and body weight were measured twice per week.

H1975 Xenograft Model. H1975 cells (10^7 cells) were injected subcutaneously into the right flank of SCID mice (8 weeks old; Charles River Laboratories). When the average tumor volume reached about 210 mm^3, animals were treated with vehicle or mobocertinib 3, 10, or 30 mg/kg once daily for 14 days. Tumor size was measured at least twice a week. Mice were euthanized on day 14 at 2, 6, or 24 hours after the last dose, when blood samples were collected for PK analysis.

Intracranial Metastases Model. Luciferase-expressing H1975 cells were generated from the parental H1975 line. Female Athymic Nude-*Foxn1*^{nu} mice were implanted intracranially with 10^5 cells in 10 μL on day 0. Treatment began on day 6 at an overall mean tumor burden of 1.5×10^6 p/s. *In vivo* bioluminescence images were acquired after injection of 150 mg/kg D-luciferin on days 6, 13, 20, 27, and 34.

In all mouse studies of tumor models, the vehicle solution for oral drug delivery was 10% N-methyl-2-pyrrolidone/90% polyethylene glycol. Stock solutions of mobocertinib were prepared in vehicle, and a constant dose volume was used to deliver mobocertinib doses ranging from 15 to 50 mg/kg.

In each of the studies, plasma levels of mobocertinib, AP32914, AP32960, and other analytes (afatinib or erlotinib) were measured using nonvalidated LC/MS methods (Supplementary Table S6).

All animal studies were approved by a local Institutional Animal Care and Use Committee (IACUC) and conducted in accordance with the regulations of the Association for Assessment and Accreditation of Laboratory Animal Care (AAALAC) and local IACUC guidelines.

SVD GEMM Model

Mouse Generation. The coding region of human *EGFR*ex20ins SVD with the Kozak sequence (GCCGCCACC) was synthesized at GENEWIZ, Inc. and introduced into pGV at the EcoRI cloning site. Sequence-confirmed human *EGFR*ex20ins SVD plasmid was coelectroporated with plasmid-expressing flippase (FLP) recombinase into mouse ES cells. Electroporated ES cells were selected with hygromycin, and positive clones were identified by PCR. Positive ES clones were injected into mouse blastocysts for chimera generation. Chimera mice were crossed with WT mice to generate mice with germline mutations. Mouse genomic DNA was used as the PCR template, and the human *EGFR*ex20ins SVD sequence was confirmed with Sanger sequencing. The genotyping primers used were DSVD-forward: TCCGTGGACAATCCCCACGT and DSVD-reverse: CAGCGTCAAT CATCCAACAC. Detailed methods for this strategy were previously described (56). All animal experiments, including breeding and treatment studies, were approved by the NYU Langone Medical Center IACUC.

Treatment and Monitoring. *EGFR*ex20ins SVD mice were monitored by MRI for tumor development after intranasal induction with adeno-Cre (5×10^7 plaque-forming units). Tumor-bearing mice were dosed with mobocertinib (30 mg/kg, orally, daily) and monitored by MRI every 2 weeks. Mice were euthanized and lung tissues were collected and fixed with 10% formalin.

Immunohistochemistry staining was performed at iHisto, Inc. using the following antibodies: anti-TTF1 5883–1 (Epitomics, Inc.), anti-p63 ab53039 (Abcam), anti-pEGFR (Tyr1068; #3777; Cell Signaling Technology), and anti-pERK1/2 (Thr202/Tyr204; #4370; Cell Signaling Technology).

Data Sharing Statement

The data sets supporting the results reported in this article will be made available within 3 months from initial request to researchers who provide a methodologically sound proposal. The data will be provided in compliance with applicable laws, data protection, and requirements for consent and anonymization.

Authors' Disclosures

F. Gonzalvez is an employee and shareholder of Aligos Therapeutics and a former employee of ARIAD. S. Vincent is an employee and shareholder of Takeda. T.E. Baker is an employee and shareholder of MOMA Therapeutics and a former employee of ARIAD. A.E. Gould is an employee of Takeda. S.D. Wardwell is an employee and shareholder of Blueprint Medicines and a former employee of ARIAD. S. Nadworny is a former employee of ARIAD. Y. Ning is a former employee of ARIAD. S. Zhang is a former employee of ARIAD and an employee and stockholder of EMD Serono, a subsidiary of Merck KGaA, Darmstadt, Germany. W-S. Huang is an employee and shareholder of Theseus Pharmaceuticals and a former employee of ARIAD. Y. Hu is an employee of Takeda. F. Li is a former employee of ARIAD. M.T. Greenfield is a former employee of ARIAD. S.G. Zech is an employee and shareholder of Amgen Inc. and a former employee of ARIAD. B. Das is a former employee of ARIAD. N.I. Narasimhan is a former employee of ARIAD. T. Clackson is an employee and shareholder of Xilio Therapeutics and is a former employee of ARIAD. D. Dalgarno is an employee and shareholder of Theseus Pharmaceuticals and a former employee of ARIAD. W.C. Shakespeare is an employee and

shareholder of Theseus Pharmaceuticals and a former employee of ARIAD. M. Fitzgerald is a former employee of Takeda. J. Chouitar is an employee of Takeda. R.J. Griffin is an employee of Takeda and a shareholder of GSK. S.K. Wong reports sponsored research agreements with Takeda, BMS, Mirati, Alkermes, Merus, Amgen, Ansun Biopharma, Enliven Therapeutics, Tvardi Therapeutics, Delfi Diagnostics, and Dracen Pharmaceuticals; a consulting agreement with Merck; and consulting and sponsored research agreements with AstraZeneca, Janssen, Pfizer/Array, Novartis, and Zentalis. X. Zhu is an employee and shareholder of Regor Pharmaceuticals, Inc. and a former employee of ARIAD. V.M. Rivera is an employee and shareholder of Theseus Pharmaceuticals and a former employee of Ariad. No disclosures were reported by the other authors.

Authors' Contributions

F. Gonzalvez: Conceptualization, data curation, formal analysis, investigation, methodology, writing-original draft, writing-review and editing. **S. Vincent:** Conceptualization, data curation, formal analysis, investigation, methodology, writing-original draft, writing-review and editing. **T.E. Baker:** Data curation, formal analysis, investigation, methodology, writing-review and editing. **A.E. Gould:** Data curation, investigation, writing-original draft, writing-review and editing. **S. Li:** Investigation, methodology, writing-review and editing. **S.D. Wardwell:** Investigation, writing-review and editing. **S. Nadworny:** Investigation, writing-review and editing. **Y. Ning:** Investigation, writing-review and editing. **S. Zhang:** Data curation, investigation, writing-review and editing. **W.-S. Huang:** Conceptualization, formal analysis, investigation, writing-review and editing. **Y. Hu:** Investigation, writing-review and editing. **F. Li:** Investigation, writing-review and editing. **M.T. Greenfield:** Investigation, writing-review and editing. **S.G. Zech:** Investigation, writing-review and editing. **B. Das:** Investigation, writing-review and editing. **N.I. Narasimhan:** Investigation, writing-review and editing. **T. Clackson:** Conceptualization, supervision, investigation, writing-review and editing. **D. Dalgarno:** Writing-review and editing. **W.C. Shakespeare:** Conceptualization, supervision, writing-review and editing. **M. Fitzgerald:** Investigation, writing-review and editing. **J. Chouitar:** Resources, investigation, writing-review and editing. **R.J. Griffin:** Writing-review and editing. **S. Liu:** Resources, investigation, methodology, writing-review and editing. **K. Wong:** Writing-review and editing. **X. Zhu:** Conceptualization, investigation, writing-review and editing. **V.M. Rivera:** Conceptualization, data curation, formal analysis, investigation, methodology, writing-original draft, writing-review and editing. NOTE: The authors define "Investigation" as performing clinical experiments and collecting data.

Acknowledgments

We thank the American Association for Cancer Research (AACR) for its financial and material support in the development of the AACR Project GENIE registry, as well as members of the consortium for their commitment to data sharing. Interpretations are the responsibility of study authors. We also thank Dr. Robert Doebele and Dr. Anh Le, University of Colorado, for the use of CUTO14 cells, and Anna Kohlmann, Paul M. Taslimi, Tianjun Zhou, Lingling Zhang, Hyun G. Jang, Emily Y. Ye, Meera Tugnait, Hua Zou, Weston Lane, Robert Skene, R. Scott Rowland, and Andy Garner for their contributions to this study. Professional medical writing assistance was provided by Lauren Gallagher, RPh, PhD, and Lela Creutz, PhD, of Peloton Advantage, LLC, an OPEN Health company, Parsippany, New Jersey, and funded by Millennium Pharmaceuticals, Inc. Teodor G. Paunescu, PhD (Millennium Pharmaceuticals, Inc., Cambridge, Massachusetts, a wholly owned subsidiary of Takeda Pharmaceutical Company Limited) is acknowledged for editorial assistance. All studies were funded by Millennium Pharmaceuticals, Inc., a wholly owned subsidiary of Takeda Pharmaceutical Company Limited.

Received November 25, 2020; revised February 5, 2021; accepted February 22, 2021; published first February 25, 2021.

REFERENCES

1. Arbour KC, Riely GJ. Systemic therapy for locally advanced and metastatic non-small cell lung cancer: a review. JAMA 2019;322:764–74.
2. Zhang YL, Yuan JQ, Wang KF, Fu XH, Han XR, Threapleton D, et al. The prevalence of EGFR mutation in patients with non-small cell lung cancer: a systematic review and meta-analysis. Oncotarget 2016;7:78985–93.
3. Barlesi F, Mazieres J, Merlio JP, Debieuvre D, Mosser J, Lena H, et al. Routine molecular profiling of patients with advanced non-small-cell lung cancer: results of a 1-year nationwide programme of the French Cooperative Thoracic Intergroup (IFCT). Lancet 2016;387:1415–26.
4. Shi Y, Au JS, Thongprasert S, Srinivasan S, Tsai CM, Khoa MT, et al. A prospective, molecular epidemiology study of EGFR mutations in Asian patients with advanced non-small-cell lung cancer of adenocarcinoma histology (PIONEER). J Thorac Oncol 2014;9:154–62.
5. Midha A, Dearden S, McCormack R. EGFR mutation incidence in non-small-cell lung cancer of adenocarcinoma histology: a systematic review and global map by ethnicity (mutMapII). Am J Cancer Res 2015;5:2892–911.
6. Sharma SV, Bell DW, Settleman J, Haber DA. Epidermal growth factor receptor mutations in lung cancer. Nat Rev Cancer 2007;7:169–81.
7. Kobayashi Y, Mitsudomi T. Not all epidermal growth factor receptor mutations in lung cancer are created equal: perspectives for individualized treatment strategy. Cancer Sci 2016;107:1179–86.
8. Arcila ME, Nafa K, Chaft JE, Rekhtman N, Lau C, Reva BA, et al. EGFR exon 20 insertion mutations in lung adenocarcinomas: prevalence, molecular heterogeneity, and clinicopathologic characteristics. Mol Cancer Ther 2013;12:220–9.
9. Oxnard GR, Lo PC, Nishino M, Dahlberg SE, Lindeman NI, Butaney M, et al. Natural history and molecular characteristics of lung cancers harboring *EGFR* exon 20 insertions. J Thorac Oncol 2013;8:179–84.
10. Mitsudomi T, Morita S, Yatabe Y, Negoro S, Okamoto I, Tsurutani J, et al. Gefitinib versus cisplatin plus docetaxel in patients with non-small-cell lung cancer harbouring mutations of the epidermal growth factor receptor (WJTOG3405): an open label, randomised phase 3 trial. Lancet Oncol 2010;11:121–8.
11. Sequist LV, Yang JC, Yamamoto N, O'Byrne K, Hirsh V, Mok T, et al. Phase III study of afatinib or cisplatin plus pemetrexed in patients with metastatic lung adenocarcinoma with EGFR mutations. J Clin Oncol 2013;31:3327–34.
12. Rosell R, Carcereny E, Gervais R, Vergnenegre A, Massuti B, Felip E, et al. Erlotinib versus standard chemotherapy as first-line treatment for European patients with advanced EGFR mutation-positive non-small-cell lung cancer (EURTAC): a multicentre, open-label, randomised phase 3 trial. Lancet Oncol 2012;13:239–46.
13. Wu YL, Cheng Y, Zhou X, Lee KH, Nakagawa K, Niho S, et al. Dacomitinib versus gefitinib as first-line treatment for patients with EGFR-mutation-positive non-small-cell lung cancer (ARCHER 1050): a randomised, open-label, phase 3 trial. Lancet Oncol 2017;18:1454–66.
14. Yu HA, Arcila ME, Rekhtman N, Sima CS, Zakowski MF, Pao W, et al. Analysis of tumor specimens at the time of acquired resistance to EGFR-TKI therapy in 155 patients with EGFR-mutant lung cancers. Clin Cancer Res 2013;19:2240–7.
15. Andrews Wright NM, Goss GD. Third-generation epidermal growth factor receptor tyrosine kinase inhibitors for the treatment of non-small cell lung cancer. Transl Lung Cancer Res 2019;8:S247–S64.

16. Ricordel C, Friboulet L, Facchinetti F, Soria JC. Molecular mechanisms of acquired resistance to third-generation EGFR-TKIs in EGFR T790M-mutant lung cancer. Ann Oncol 2018;29:i28–37.
17. Zhou W, Ercan D, Chen L, Yun CH, Li D, Capelletti M, et al. Novel mutant-selective EGFR kinase inhibitors against EGFR T790M. Nature 2009;462:1070–4.
18. Boehringer Ingelheim Pharmaceuticals, Inc. Gilotrif [package insert]. Ridgefield, CT: Boehringer Ingelheim Pharmaceuticals, Inc.; 2019.
19. Cho JH, Lim SH, An HJ, Kim KH, Park KU, Kang EJ, et al. Osimertinib for patients with non-small-cell lung cancer harboring uncommon EGFR mutations: a multicenter, open-label, phase II trial (KCSG-LU15–09). J Clin Oncol 2020;38:488–95.
20. Vyse S, Huang PH. Targeting *EGFR* exon 20 insertion mutations in non-small cell lung cancer. Signal Transduct Target Ther 2019;4:5.
21. Riess JW, Gandara DR, Frampton GM, Madison R, Peled N, Bufill JA, et al. Diverse EGFR exon 20 insertions and co-occurring molecular alterations identified by comprehensive genomic profiling of NSCLC. J Thorac Oncol 2018;13:1560–8.
22. Yang JC, Sequist LV, Geater SL, Tsai CM, Mok TS, Schuler M, et al. Clinical activity of afatinib in patients with advanced non-small-cell lung cancer harbouring uncommon *EGFR* mutations: a combined post-hoc analysis of LUX-Lung 2, LUX-Lung 3, and LUX-Lung 6. Lancet Oncol 2015;16:830–8.
23. Naidoo J, Sima CS, Rodriguez K, Busby N, Nafa K, Ladanyi M, et al. Epidermal growth factor receptor exon 20 insertions in advanced lung adenocarcinomas: Clinical outcomes and response to erlotinib. Cancer 2015;121:3212–20.
24. Yasuda H, Park E, Yun CH, Sng NJ, Lucena-Araujo AR, Yeo WL, et al. Structural, biochemical, and clinical characterization of epidermal growth factor receptor (EGFR) exon 20 insertion mutations in lung cancer. Sci Transl Med 2013;5:216ra177.
25. Lee Y, Kim TM, Kim DW, Kim S, Kim M, Keam B, et al. Preclinical modeling of osimertinib for NSCLC with EGFR exon 20 insertion mutations. J Thorac Oncol 2019;14:1556–66.
26. Piotrowska Z, Fintelmann FJ, Sequist LV, Jahagirdar B. Response to osimertinib in an EGFR exon 20 insertion-positive lung adenocarcinoma. J Thorac Oncol 2018;13:e204–e6.
27. Piotrowska Z, Wang Y, Sequist LV, Ramalingam SS. ECOG-ACRIN 5162: a phase II study of osimertinib 160 mg in NSCLC with EGFR exon 20 insertions [abstract]. J Clin Oncol 2020;38:9513.
28. Riess J, Floch N, Martin M, Orme J, Staniszewska A, Menard L, et al. Antitumor activity of osimertinib in NSCLC harboring EGFR exon 20 insertions [abstract]. J Clin Oncol 2017;35:9030.
29. Vasconcelos PENS, Gergis C, Viray H, Varkaris A, Fujii M, Rangachari D, et al. EGFR-A763_Y764insFQEA is a unique exon 20 insertion mutation that displays sensitivity to approved and in-development lung cancer EGFR tyrosine kinase inhibitors. JTO Clin Res Rep 2020; 1:100051.
30. Luo YH, Chen YM. Recent advances in the development of mutant-selective EGFR inhibitors for non-small cell lung cancer patients with EGFR-TKI resistance. Transl Lung Cancer Res 2014;3:368–9.
31. Carey KD, Garton AJ, Romero MS, Kahler J, Thomson S, Ross S, et al. Kinetic analysis of epidermal growth factor receptor somatic mutant proteins shows increased sensitivity to the epidermal growth factor receptor tyrosine kinase inhibitor, erlotinib. Cancer Res 2006;66: 8163–71.
32. Mulloy R, Ferrand A, Kim Y, Sordella R, Bell DW, Haber DA, et al. Epidermal growth factor receptor mutants from human lung cancers exhibit enhanced catalytic activity and increased sensitivity to gefitinib. Cancer Res 2007;67:2325–30.
33. Hirano T, Yasuda H, Tani T, Hamamoto J, Oashi A, Ishioka K, et al. In vitro modeling to determine mutation specificity of EGFR tyrosine kinase inhibitors against clinically relevant EGFR mutants in non-small-cell lung cancer. Oncotarget 2015;6:38789–803.
34. Lacouture ME. Mechanisms of cutaneous toxicities to EGFR inhibitors. Nat Rev Cancer 2006;6:803–12.
35. Mascia F, Lam G, Keith C, Garber C, Steinberg SM, Kohn E, et al. Genetic ablation of epidermal EGFR reveals the dynamic origin of adverse effects of anti-EGFR therapy. Sci Transl Med 2013;5:199ra10.
36. Lichtenberger BM, Gerber PA, Holcmann M, Buhren BA, Amberg N, Smolle V, et al. Epidermal EGFR controls cutaneous host defense and prevents inflammation. Sci Transl Med 2013;5:199ra11.
37. Huang WS, Metcalf CA, Sundaramoorthi R, Wang Y, Zou D, Thomas RM, et al. Discovery of 3-[2-(imidazo[1,2-b]pyridazin-3-yl)ethynyl]-4-methyl-N-{4-[(4-methylpiperazin-1-yl)methyl]-3-(trifluoromethyl) phenyl}benzamide (AP24534), a potent, orally active pan-inhibitor of breakpoint cluster region-abelson (BCR-ABL) kinase including the T315I gatekeeper mutant. J Med Chem 2010;53:4701–19.
38. AACR Project GENIE Consortium. AACR Project GENIE: powering precision medicine through an international consortium. Cancer Discov 2017;7:818–31.
39. Robichaux JP, Elamin YY, Tan Z, Carter BW, Zhang S, Liu S, et al. Mechanisms and clinical activity of an EGFR and HER2 exon 20-selective kinase inhibitor in non-small cell lung cancer. Nat Med 2018;24:638–46.
40. Vasconcelos PENS, Kobayashi IS, Kobayashi SS, Costa DB. Preclinical characterization of mobocertinib highlights the putative therapeutic window of this novel EGFR inhibitor to EGFR exon 20 insertion mutations. JTO Clin Res Rep 2021;2:100105.
41. Riely GJ, Neal JW, Camidge DR, Spira A, Piotrowska Z, Horn L, et al. Updated results from a phase I/II study of mobocertinib (TAK-788) in NSCLC with EGFR exon 20 insertions (exon20ins) [abstract 1261MO]. Ann Oncol 2020;31:S815–S6.
42. Hasegawa H, Yasuda H, Hamamoto J, Masuzawa K, Tani T, Nukaga S, et al. Efficacy of afatinib or osimertinib plus cetuximab combination therapy for non-small-cell lung cancer with EGFR exon 20 insertion mutations. Lung Cancer 2019;127:146–52.
43. van Veggel B, Madeira R Santos JFV, Hashemi SMS, Paats MS, Monkhorst K, Heideman DAM, et al. Osimertinib treatment for patients with *EGFR* exon 20 mutation positive non-small cell lung cancer. Lung Cancer 2020;141:9–13.
44. Udagawa H, Hasako S, Ohashi A, Fujioka R, Hakozaki Y, Shibuya M, et al. TAS6417/CLN-081 is a pan-mutation-selective EGFR tyrosine kinase inhibitor with a broad spectrum of preclinical activity against clinically relevant EGFR mutations. Mol Cancer Res 2019;17:2233–43.
45. Xu Y, Zhang L, Zhu L, Wang Y, Wang M, Yang Z. DZD9008, an oral, wild type selective EGFR inhibitor for the treatment of non-small-cell lung cancer with Exon20 insertion and other activating mutations [abstract]. Cancer Res 2019;79:3081.
46. Liu SV, Villaruz LC, Lee VHF, Zhu VW, Baik CS, Sacher A, et al. First analysis of RAIN-701: Study of tarloxotinib in patients with non-small cell lung cancer (NSCLC) EGFR Exon 20 insertion, HER2-activating mutations & other solid tumours with NRG1/ERBB gene fusions [abstract LBA61]. Ann Oncol 2020;31(suppl 4):S1189.
47. Nagamoto Y, Miyamoto M, Togashi N, Taira T, Jimbo T, Isoyama T, et al. Preclinical evaluation of DS-2087b, a novel and selective inhibitor of EGFR/HER2 exon 20 insertions [abstract 11P]. Ann Oncol 2020;31(suppl 4):S248.
48. Le X, Goldman JW, Clarke JM, Tchekmedyian N, Piotrowska Z, Chu D, et al. Poziotinib shows activity and durability of responses in subgroups of previously treated EGFR exon 20 NSCLC patients [abstract]. J Clin Oncol 2020;38:9514.
49. Prelaj A, Bottiglieri A, Proto C, Lo Russo G, Signorelli D, Ferrara R, et al. Poziotinib in advanced NSCLC with EGFR or HER2 exon 20 insertion mutation: Initial results from a single site expanded access program [abstract 1388P]. Ann Oncol 2020;31(suppl 4):S882.
50. Yun J, Lee SH, Kim SY, Jeong SY, Kim JH, Pyo KH, et al. Antitumor activity of amivantamab (JNJ-61186372), an EGFR-MET bispecific antibody, in diverse models of EGFR exon 20 insertion-driven NSCLC. Cancer Discov 2020;10:1194–209.
51. Park K, John T, Kim S, Lee JS, Shu CA, Kim D, et al. Amivantamab (JNJ-61186372), an anti-EGFR-MET bispecific antibody, in patients with EGFR exon 20 insertion (exon20ins)-mutated non-small cell lung cancer (NSCLC) [abstract]. J Clin Oncol 2020;38:9512.
52. Sabari JK, Shu CA, Park K, Leighl N, Mitchell PL, Kim S, et al. Amivantamab in post-platinum EGFR exon 20 insertion mutant non-small cell lung cancer [abstract OA04.04]. Presented at: Annual Meeting of the World Conference on Lung Cancer (WCLC 2020-Virtual), January 28–31, 2021.

53. Riely GJ, Neal JW, Camidge DR, Spira AI, Piotrowska Z, Costa DB, et al. Activity and safety of mobocertinib (TAK-788) in previously treated non–small cell lung cancer with EGFR exon 20 insertion mutations from a phase I/II trial. Cancer Discov 2021;11:1688–99.
54. Manning G, Whyte DB, Martinez R, Hunter T, Sudarsanam S. The protein kinase complement of the human genome. Science 2002;298:1912–34.
55. Chartier M, Chénard T, Barker J, Najmanovich R. Kinome Render: a stand-alone and web-accessible tool to annotate the human protein Kinome tree. PeerJ 2013;1:e126.
56. Akbay EA, Moslehi J, Christensen CL, Saha S, Tchaicha JH, Ramkissoon SH, et al. D-2-hydroxyglutarate produced by mutant IDH2 causes cardiomyopathy and neurodegeneration in mice. Genes Dev 2014;28:479–90.